Analyst

RSC Publishing

PAPER

View Article Online
View Journal | View Issue

Cite this: *Analyst*, 2013, **138**, 2877

Controllable synthesis of silver nanoparticle-decorated reduced graphene oxide hybrids for ammonia detection†

Shumao Cui, Shun Mao, Zhenhai Wen, Jingbo Chang, Yang Zhang and Junhong Chen*

Received 28th December 2012
Accepted 7th March 2013

DOI: 10.1039/c3an36922f

www.rsc.org/analyst

We demonstrate controllable fabrication of Ag nanoparticle (NP)-decorated reduced graphene oxide (RGO/Ag) hybrids and their application for fast and selective detection of ammonia at room temperature. Ag NPs greatly improved the sensitivity of RGO. The response time (6 s) and recovery time (10 s) are comparable with our previous Ag NP-decorated multiwalled carbon nanotube (MWCNT/Ag) NH_3 sensors; however, the sensitivity is about twice that of MWCNT/Ag hybrids. We found that the loading density of NPs greatly affects the sensing performance of RGO/Ag hybrids and a proper NP loading leads to maximum sensitivity.

Introduction

In recent years many research breakthroughs have been achieved on graphene, which is a two-dimensional single layer of graphite. Because of its unique structure and superior thermal, mechanical, and electric properties,[1,2] such as high charge mobility, graphene has been applied to various applications, including sensors,[3–7] photodetectors, and lithium-ion batteries.[8,9] Graphene is sensitive to changes in chemical environments due to its high charge mobility, high specific surface area, and low electrical noise at room temperature;[10] however, the low sensitivity and poor selectivity of intrinsic graphene limit its use in gas-sensing applications.[10,11] Fortunately, it is well-known that noble metals, such as Au, Pd, and Pt, have been widely used as catalysts and deposited onto carbon nanotubes, forming hybrid structures for highly selective and sensitive gas sensors. For example, Au is highly active for CO oxidation and has been deposited on carbon nanotubes for selective CO detection.[12,13]

Recently, many nanohybrids composed of graphene and noble metals have been prepared and their high room-temperature sensing performance has been reported;[14,15] as such, noble-metal decorated graphene nanohybrids are expected to be a new type of sensing material with high sensitivity and excellent selectivity. Furthermore, it was reported that Pt-decorated graphene is much more sensitive than Pt-decorated multiwalled carbon nanotubes (MWCNTs) for hydrogen detection, which explains the superior properties of graphene in gas-sensing applications.[16] In our previous study, a fast and selective room-temperature ammonia (NH_3) sensor was synthesized using Ag NP-decorated MWCNTs.[17] Based on our experimental and theoretical results, the Ag NP coating greatly improved the sensing performance of MWCNTs toward NH_3; therefore, it is anticipated that Ag NP-decorated graphene could offer improved NH_3 sensing properties over bare graphene.

Here we report on a Ag NP-decorated reduced graphene oxide (RGO) hybrid (RGO/Ag) sensing platform and its sensing properties for NH_3 detection before and after the deposition of Ag NPs. RGO was synthesized by a top-down method, chemically reducing graphene oxide (GO) obtained by chemical exfoliation of graphite, which is inexpensive and one of the scalable methods to fabricate graphene.[10] Silver NPs were deposited on RGO by physical vapor deposition using a mini-arc plasma as a source with low contamination, and the amount of Ag NPs on the RGO surface was controlled by the deposition time. Based on the results, the Ag NP coating dramatically improved the sensitivity; by comparison, the sensitivity of RGO/Ag is higher than that of RGO and MWCNT/Ag. The influence of Ag NP loading on the sensing performance of RGO/Ag hybrids was studied. The low-cost assembly of Ag NPs onto the RGO surface using a simple physical vapor deposition process holds great potential for large-scale applications.

Experimental

Preparation of RGO

The RGO was obtained by chemically reducing GO dispersion, which was prepared using a modified Hummers method.[18] Briefly, $H_3NO{\cdot}HCl$ was added into the GO dispersion and the mixture was continuously stirred at 80 °C for 30 hours. Then,

Department of Mechanical Engineering, University of Wisconsin-Milwaukee, 3200 N Cramer Street, Milwaukee, WI, 53211, USA. E-mail: jhchen@uwm.edu; Fax: +1-414-229-6958; Tel: +1-414-229-2615

† Electronic supplementary information (ESI) available: Supplemental figures. See DOI: 10.1039/c3an36922f

the black product was filtered and washed with distilled water and acetone to obtain RGO powders. Finally, the RGO dispersion was prepared by distributing the RGO powders in *N*,*N*-dimethylformamide (DMF) with sonication for 2 hours.

Sensor fabrication and characterization

Scheme 1 illustrates the complete sensor fabrication process. Interdigitated gold electrodes were fabricated using e-beam lithography on a silicon substrate with a SiO_2 thin top layer. Then, a tiny drop (1 μl) of RGO dispersion was drop-cast on the gold electrodes, and RGO flakes bridged the gold fingers after solvent evaporation. The amount of RGO flakes on gold electrodes can be controlled by adjusting the dispersion concentration. Further annealing treatment at 200 °C for 1 hour in Ar flow (1 l min^{-1}) was performed to remove the residual DMF and improve the contacts between the RGO and gold electrodes.

To synthesize the RGO/Ag hybrid, we produced Ag NPs using a previously reported physical vapor deposition process in a mini-arc plasma reactor.[17,19] The mini-arc plasma was generated between two carbon electrodes driven by a commercial tungsten inert gas (TIG) arc welder (Miller Maxstar 150 STH), and small pieces of Ag (99.999% purity) cut from an Ag wire were used as the source material. The Ag pieces were first vaporized by the mini-arc plasma source. Then, the Ag vapor was carried by an Ar flow downstream and quenched in the gas phase, forming Ag NPs. The as-produced Ag NPs were directly deposited onto the RGO supported by gold electrodes or a transmission electron microscopy (TEM) grid using an electrostatic force-directed assembly (ESFDA) process.[20]

The as-produced RGO was characterized in our previous report.[18] The morphology and crystal structure of the RGO/Ag hybrid were studied using a field-emission scanning electron microscope (SEM) (Hitachi S4800) and a high-resolution transmission electron microscope (HRTEM) (Hitachi H-9000-NAR) with 0.18 nm point and 0.11 nm lattice resolution operated at an accelerating voltage of 300 kV. The surface chemical composition was characterized by an X-ray photoelectron spectroscope (XPS) (HP 5950A). Raman spectra were taken using a Raman spectrometer (Renishaw 1000B).

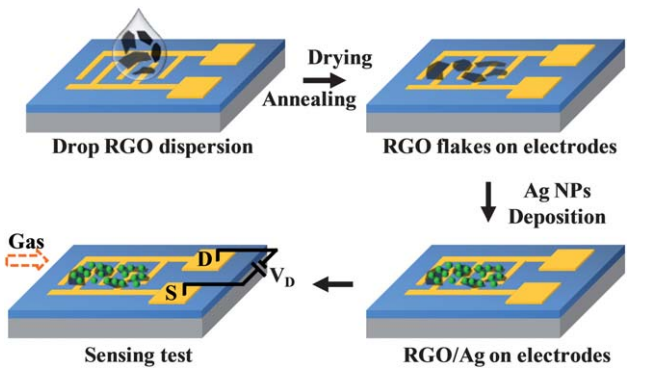

Scheme 1 Schematic illustration of the process to fabricate RGO/Ag hybrid sensor devices and the subsequent sensing measurements.

Ammonia-sensing measurement

The sensor device was placed in an air-tight chamber with electrical feedthroughs. A constant voltage was added to the electrodes, and the variation of resistance was monitored and recorded with the changes in the gas environment using a Keithley 2602 source meter. Typically, a sensing-measurement cycle has three continuous steps: (1) introducing dry air (2 l min^{-1}) as a background, then (2) injecting ammonia gas (2 l min^{-1}) to register a sensing signal, and (3) introducing dry air (2 l min^{-1}) again for sensor recovery.

Results and discussion

After the RGO dispersion dried on the gold electrode, the morphology was characterized by SEM. Fig. 1a shows an SEM image of one typical RGO flake bridging a pair of gold electrode fingers in a sensor device; the wrinkle on the RGO flake is an intrinsic characteristic.[21] After *in situ* deposition of Ag NPs on RGO, RGO/Ag hybrids formed on the device (Fig. 1b); it is evident that Ag NPs distribute uniformly on the RGO surface. Since the number of Ag NPs can be controlled by the deposition time, the loading density shown in Fig. 1b is relatively high for a deposition time of 15 min. The RGO/Ag hybrids were also characterized by TEM with a sample prepared on a TEM grid. Fig. 1c shows a TEM image of RGO/Ag hybrids suspended over the carbon film hole. The size of the Ag NPs ranges from several nanometers to 10 nm over the RGO surface. Some larger NPs of about 20 nm anchor on the edge due to the stronger electrostatic force during the ESFDA process.[20] The inset in Fig. 1c is an SAED pattern of RGO/Ag hybrids, evidencing a single layer of RGO and good crystallinity of Ag NPs, in which the first four bright continuous rings are indexed to cubic fcc (111), (200), (220), and (311) lattice planes of Ag metal from the inside to the

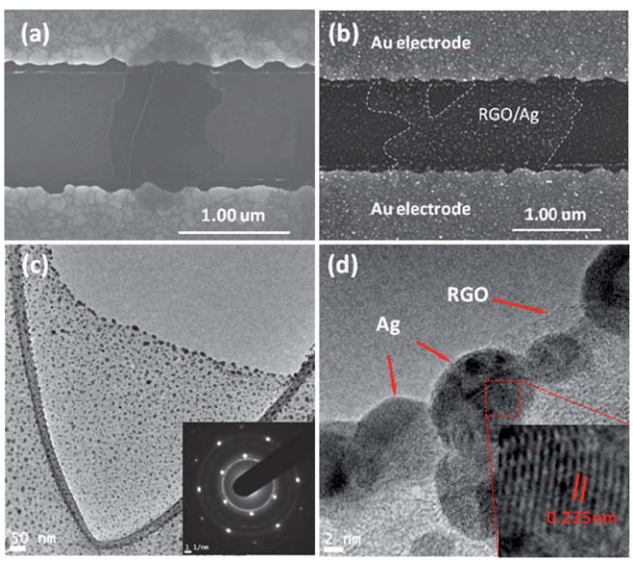

Fig. 1 (a and b) SEM images of an RGO flake before and after Ag NP deposition bridging a pair of gold electrode fingers. (c) TEM image of an RGO flake decorated with Ag NPs. The inset is an SAED pattern of RGO/Ag hybrids. (d) HRTEM image of RGO/Ag hybrids.

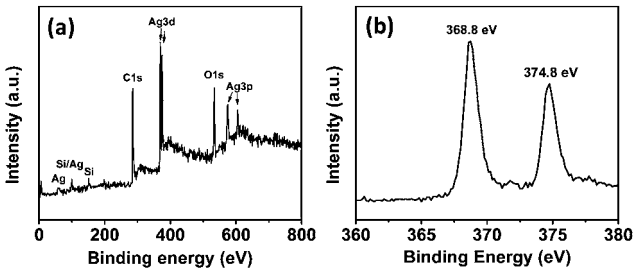

Fig. 2 (a) XPS spectra of RGO/Ag hybrids. (b) High-resolution XPS spectra of Ag 3d from RGO/Ag hybrids.

outside.[17] An HRTEM image (Fig. 1d) further confirms the crystalline structure of Ag NPs, and the measured lattice spacing of 0.235 nm is indexed to the (111) plane of Ag.

The surface composition of the RGO/Ag hybrid nanostructure was examined using XPS (Fig. 2). The entire XPS survey spectra (Fig. 2a) clearly show C 1s, O 1s, Ag 3d, and Ag 3p peaks, indicating that the hybrids consist of C, O, and Ag elements. The Si peak in the spectra is from the silicon wafer, which was used as the support in the test. According to our previous study, RGO mainly contributes to the C 1s and O 1s signals detected due to the graphene basal plane and the oxygen-containing functional groups.[18] A part of the O signal could be from the oxygen adsorption of air. It was reported that Ag 3d peaks of Ag NPs were composed of Ag metal and Ag^+ appeared at 368.3 and 374.3 eV.[22] In our study, the Ag 3d peaks are centered at 368.8 and 374.8 eV (Fig. 2b), which are close to the reported results, indicating metallic Ag and Ag^+ on the RGO surface. This is also consistent with our theoretical calculation results that the surface of Ag NPs is likely oxidized by oxygen when exposed to air.[19] The RGO/Ag hybrids were also characterized using Raman spectroscopy. Fig. S1† shows the Raman spectra of RGO before and after the Ag NP decoration. The spectrum of RGO, with a D band to G band intensity ratio of 1.26, is consistent with that of chemically reduced graphene oxide.[23] The similar spectra of RGO with and without the Ag NP decoration indicate that Ag NPs do not significantly modify the structure of RGO.

Fig. 3a shows the electrical characteristics of a field-effect transistor (FET) device based on RGO/Ag hybrids. The straight linear *I–V* curve indicates that the contacts between the RGO/Ag and gold electrodes are ohmic. To investigate the effect of Ag NPs on RGO, the resistance of the device was measured before and after the deposition of Ag NPs. We found the resistance of this sample increased from 1.3×10^3 to 1.4×10^3 Ω, which is the typical trend for all samples. Because the RGO in this study is a p-type semiconductor (Fig. S2†), the increased resistance could be explained by the fact that Ag NPs led to hole depletion zones in their interface between the RGO and Ag NPs, which is consistent with our previous results of depositing SnO_2 NPs on RGO sheets.[24] However, the resistance of MWCNTs decreased when Ag NPs were deposited on them (MWCNTs are p-type semiconductors, the same as RGO), possibly because of the oxygen-containing functional groups on RGO. The inset in Fig. 3a shows the source–drain current curve of gate voltage dependence for the FET device, which demonstrates that the

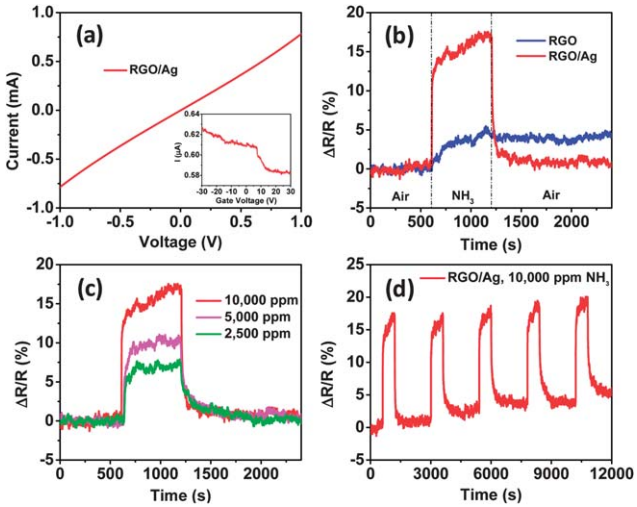

Fig. 3 (a) *I–V* characteristic of RGO/Ag hybrids on gold electrodes and the inset is the FET measurement of the sensor device. (b) The room-temperature dynamic-sensing responses of RGO before and after Ag NP deposition. (c) Dynamic responses of RGO/Ag hybrids when exposed to different concentrations of NH_3. (d) Five-cycle responses of RGO/Ag to 10 000 ppm NH_3, indicating a good stability of the sensor.

current decreases slowly with gate voltage sweeping from −30 to 30 V, indicating that the RGO/Ag hybrids are p-type semiconductors and the Ag NPs did not change the semiconducting type of RGO.

To demonstrate the sensing enhancement of Ag NPs, the sensing performance of RGO was measured before and after Ag NP deposition, respectively. To ensure comparable results, bare RGO was first tested against NH_3. Then, the same sensor was tested again after depositing Ag NPs using the same sensing process. The dynamic sensing responses of both bare RGO and RGO/Ag hybrids to 10 000 ppm NH_3 are shown in Fig. 3b. The sensitivity is defined as the ratio of resistance change with exposure to the test gas to the initial resistance in air ($\Delta R/R$). The results demonstrate that the sensitivity increased from 5.1 ± 0.2% for RGO to 17.4 ± 0.2% for RGO/Ag hybrids with the same exposure time, which clearly indicates the significant sensing enhancement of Ag NPs. This enhancement also can be presented in terms of signal-to-noise ratio (S/N) of RGO and RGO/Ag hybrids. Here, S is defined as the ratio of maximum sensitivity upon NH_3 exposure to the average sensitivity in air before NH_3 exposure. N is defined as the ratio of maximum sensitivity in air to the average sensitivity in air in the first sensing cycle. According to the analysis, the S/N values are 7.6 and 13.6 for RGO and RGO/Ag hybrids, respectively, which suggests that RGO/Ag hybrids are better than RGO for NH_3 detection.

According to our previous study, Ag NPs act as the dominant active adsorption sites for NH_3 and enhance the sensitivity of p-type MWCNTs by "electronic sensitization."[17] NH_3 is a typical reducing gas, acting as an electron donor upon interaction with sensors. A net charge transfer from NH_3 to Ag was observed upon adsorption that reduced the oxidation state of Ag,[17] increased the hole depletion zones in RGO, and increased RGO sensitivity. Ag NP deposition on RGO resulted in more active

adsorption sites and stronger adsorption ability for NH_3, which may be responsible for the significant sensing enhancement.

The sensitivity of RGO/Ag hybrids is also about twice that of hybrids composed of MWCNTs and Ag NPs (9%) with the same deposition time.[17] The sensor's high sensitivity can be attributed to the large specific surface area of RGO, which offers more surface for Ag NP dispersion and leads to more active sites for NH_3 adsorption. The results are consistent with a previous report that demonstrated Pt-decorated graphene sensors are more sensitive than Pt-decorated MWCNTs to H_2.[16] Other properties of RGO may also play an important role in the enhancement, such as high carrier mobility (15 000 $cm^2\ V^{-1}\ s^{-1}$).[2]

To compare the response time of RGO before and after Ag NP deposition, a response time was defined as the time needed for a sensor to change more than 63.2% of the maximum sensitivity, corresponding with a one-time constant in a first-order dynamic system.[25] Analysis of Fig. 3b shows that the response times are 151 s and 6 s for RGO and RGO/Ag hybrids, respectively. The response time for RGO/Ag hybrids is comparable with that of Ag NP-decorated MWCNTs (7 s)[17] and other fast NH_3 sensors, such as an ultrafast room-temperature NH_3 sensor made of RGO (10 s).[26] The dramatically improved response by Ag NPs can be understood using a similar mechanism with Ag NPs on MWCNTs.[17] RGO has a much higher carrier mobility and acts as a conducting channel in the sensor device. The electronic state of RGO can be rapidly changed by the oxidation state of Ag NPs. Both the adsorption of NH_3 on Ag NPs and the electron transfer between NH_3 and Ag are fast, as shown in our previous study.[17] Thus, the adsorption of NH_3 can rapidly change the carrier density of RGO and lead to a faster response.

The recovery time of RGO was also improved by Ag NPs. Here, the recovery time was defined as the time needed to recover more than 63.2% of the maximum sensitivity. An analysis of Fig. 3b demonstrates that an RGO/Ag sensor can fully recover to its initial state within 6.7 min, which is comparable with that of Ag NP-decorated MWCNT hybrids (7 min).[17] However, it took the RGO overnight or days to obtain full recovery, which is consistent with previous reports.[11,27] For our RGO/Ag sensor, the recovery time is 10 s, which is also comparable with that of an Ag NP-decorated MWCNTs ammonia sensor (15 s).[17] Therefore, the recovery speed was greatly accelerated by coating with Ag NPs. The long recovery time for the RGO could be attributed to high binding energy between NH_3 molecules and RGO defects and oxygen-containing functional groups. Nevertheless, Ag NPs occupied those active sites and the direct interaction between NH_3 and Ag NPs dominated the sensing process. The rapid recovery speed indicates that the desorption barrier from the Ag surface for NH_3 molecules is low and the electron transfer from Ag to NH_3 occurs quickly, which agrees with our previous study.[17] For practical use, a sensor should have distinguishable responses to different gas concentrations. In this study, different concentrations of NH_3 were measured using the same sensor device, and the results suggest that the sensor was sensitive to concentration variations; the sensitivity increased from 7.7 $\pm$ 0.2% to 17.4 $\pm$ 0.2% with increasing gas concentrations ranging from 2500 to 10 000 ppm (Fig. 3c). To study the sensing stability, five sensing cycles were measured to 10 000 ppm NH_3 using the same sensing process (Fig. 3d). The sensing responses appear to be quite repeatable.

According to the results, Ag NPs on the RGO surface serve as the dominating sensing element; therefore, the NP density can significantly affect the sensing performance. To investigate the influence, the sensing response was measured for one sensor device with four Ag NP loadings of 5 min, 10 min, 15 min, and 20 min deposition times, respectively. First, the sensing performance was tested with Ag NPs with 5 min deposition time. Then, the same sensor was measured again with another 5 min Ag NP deposition, and this process continued until coating for 20 min deposition time. Fig. S3† shows SEM images of the sensor with different Ag NP loadings. The areal density of Ag NPs increases with increasing deposition time, and the Ag NPs distributed uniformly over the entire surface of the RGO, even with a large number of NPs, which is superior to the wet-chemical method that typically causes Ag NP aggregation with an overly high loading.[22] The sensing responses indicate that the sensitivity of RGO was dependent on Ag NP density (Fig. 4). The RGO loaded with Ag NPs with 15 min deposition time provided the highest sensitivity due to more adsorption sites, whereas longer deposition time (20 min) dramatically decreased the sensitivity, which is consistent with that of Pt-coated RGO.[28] A possible reason for this is related to the high density of Ag NPs on the RGO surface, in which a continuous Ag film formed on the RGO. To further confirm this, a bare gold electrode without RGO was deposited with Ag NPs for 1 h and the morphology was observed using SEM (Fig. S4†). The electrical test showed that the electrode gap was still open, suggesting a non-continuous Ag NP film. Until now, it is unclear why the sensitivity dramatically decreased, and more work is needed to obtain a clear understanding. Nevertheless, a proper loading of Ag NPs with about a 15 min deposition time could provide a maximum sensitivity.

The response of the RGO sensors before and after Ag NP deposition was also evaluated against NO_2, because of its strong cross-sensitivity for RGO.[18,29] Fig. 5a clearly demonstrates that the resistance change of RGO during exposure to NO_2 decreased

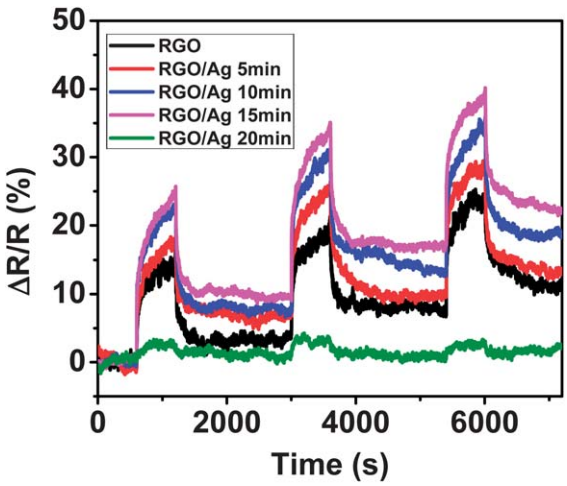

Fig. 4 Dynamic sensing response evolution of RGO with different loadings of Ag NPs.

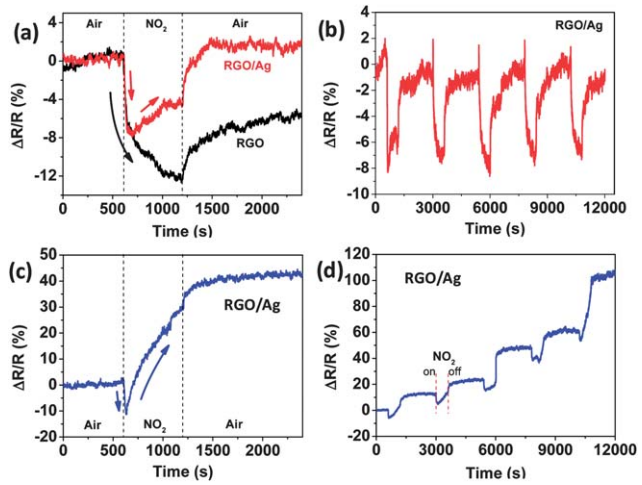

Fig. 5 (a) Dynamic sensing responses of RGO to NO_2 before and after Ag NP deposition. (b) Five-cycle sensing behavior of RGO/Ag hybrids followed by the first cycle in (a). (c and d) First cycle and the subsequent five-cycle sensing response, respectively, for another RGO/Ag sample with the same Ag NP loading (15 min deposition).

due to coating Ag NPs and led to a highly selective ammonia sensor. Interestingly, the sensitivity (real value in Fig. 5a) kept decreasing for the RGO sensor when exposed to NO_2; however, the sensitivity of the RGO/Ag hybrids rapidly decreased for a short time, and then gradually increased in NO_2 flow. For recovery in air, the RGO recovered only a part of the entire resistance change in 20 min, but RGO/Ag hybrids recovered and exceed the resistance change for NO_2 exposure in 5 min. The following five-cycle response to NO_2 was stable and can recover to its initial state in a short time (Fig. 5b), and the sensitivity is similar to the first cycle. In this study, to the best of our knowledge, this interesting over-recovery of RGO-based gas sensors is the first to be reported. To further verify this behavior, another RGO/Ag sample was prepared and tested using the same process. The sensing response to NO_2 is similar to that in Fig. 5a, but the sensitivity greatly increased for the rising part when exposed to NO_2, demonstrating an even higher over-recovery (Fig. 5c). This behavior remained the same in the next several cycles, as shown in Fig. 5d. To demonstrate the sensing behavior to NH_3, the same sensor was measured with 10 000 ppm NH_3 for five cycles (Fig. S5†); the results indicate good sensing, similar to that in Fig. 3d.

Generally, NO_2 is an oxidizing gas and withdraws electrons upon adsorption in the gas-sensing process. Ag NPs were found to improve the response of MWNCTs to NO_2.[19] It is reasonable that the resistance of the RGO/Ag hybrids decreased at the beginning, as indicated in Fig. 5a and c, due to its p-type semiconducting property and an electron transfer from the hybrids to NO_2. However, the resistance increased in the following major time for NO_2 exposure, suggesting that electrons transferred into the RGO/Ag hybrids. The large increase in resistance shown in Fig. 5c indicates an even larger number of electrons transferring from the gas to the hybrids, and NO_2 acted like an electron donor. This could be related to the intrinsic property change of RGO by decorating NPs. A similar interesting sensing-response behavior also occurred to SnO_2 NP-decorated RGO hybrids for H_2 detection. Hydrogen is a reducing gas and donates electrons into sensors upon adsorption on SnO_2-decorated p-type semiconducting MWCNTs.[30] However, the resistance of SnO_2 NP-decorated RGO hybrids decreased after exposure to H_2, suggesting that electrons transferred out of the RGO, which is the conducting channel for the sensors.[31] Because of the possible property change, the real resistance of RGO/Ag hybrids decreased less than pure RGO with the same NO_2 exposure due to fewer electrons transferring out of the RGO/Ag hybrids. Further study is warranted to obtain a clear understanding of such a phenomenon.

Conclusions

We fabricated new ammonia sensors using Ag NP-decorated RGO hybrid nanostructures in a simple and controllable fashion. The RGO/Ag hybrid sensors show a higher sensitivity than RGO alone. Ag NP decoration on RGO also achieves a fast response and recovery speed towards NH_3. The density of Ag NPs affects the sensing sensitivity, and there is a maximum sensitivity for a proper loading density. Ag NPs also decrease the response (reduced resistance) to NO_2, resulting in a better selectivity of RGO to NH_3.

Acknowledgements

The authors acknowledge financial support from the National Science Foundation (CMMI-0900509). The SEM imaging was conducted at the UWM Bioscience Electron Microscope Facility, and TEM analyses were conducted in the UWM Physics HRTEM Laboratory. Sensor electrodes were fabricated at CNM of Argonne National Laboratory, supported by U.S. DOE (DE-AC02-06CH11357).

Notes and references

1 A. K. Geim, *Science*, 2009, **324**, 1530.
2 A. K. Geim and K. S. Novoselov, *Nat. Mater.*, 2007, **6**, 183.
3 S. Alwarappan, S. Boyapalle, A. Kumar, C. Z. Li and S. Mohapatra, *J. Phys. Chem. C*, 2012, **116**, 6556.
4 S. Alwarappan, A. Erdem, C. Liu and C. Z. Li, *J. Phys. Chem. C*, 2009, **113**, 8853.
5 S. Alwarappan, R. K. Joshi, M. K. Ram and A. Kumar, *Appl. Phys. Lett.*, 2010, **96**, 263702.
6 S. Alwarappan, C. Liu, A. Kumar and C. Z. Li, *J. Phys. Chem. C*, 2010, **114**, 12920.
7 S. Alwarappan, S. R. Singh, S. Pillai, A. Kumar and S. Mohapatra, *Anal. Lett.*, 2012, **45**, 746.
8 K. S. Novoselov, V. I. Fal'ko, L. Colombo, P. R. Gellert, M. G. Schwab and K. Kim, *Nature*, 2012, **490**, 192.
9 D. A. C. Brownson and C. E. Banks, *Analyst*, 2010, **135**, 2768.
10 F. Yavari and N. Koratkar, *J. Phys. Chem. Lett.*, 2012, **3**, 1746.
11 F. Schedin, A. K. Geim, S. V. Morozov, E. W. Hill, P. Blake, M. I. Katsnelson and K. S. Novoselov, *Nat. Mater.*, 2007, **6**, 652.
12 A. S. K. Hashmi and G. J. Hutchings, *Angew. Chem., Int. Ed.*, 2006, **45**, 7896.

13 N. Du, H. Zhang, X. Y. Ma and D. Yang, *Chem. Commun.*, 2008, 6182.
14 C. Xu, X. Wang and J. W. Zhu, *J. Phys. Chem. C*, 2008, **112**, 19841.
15 J. L. Johnson, A. Behnam, S. J. Pearton and A. Ural, *Adv. Mater.*, 2010, **22**, 4877.
16 A. Kaniyoor, R. I. Jafri, T. Arockiadoss and S. Ramaprabhu, *Nanoscale*, 2009, **1**, 382.
17 S. M. Cui, H. H. Pu, G. H. Lu, Z. H. Wen, E. C. Mattson, C. Hirschmugl, M. Gajdardziska-Josifovska, M. Weinert and J. H. Chen, *ACS Appl. Mater. Interfaces*, 2012, **4**, 4898.
18 S. Mao, K. H. Yu, S. M. Cui, Z. Bo, G. H. Lu and J. H. Chen, *Nanoscale*, 2011, **3**, 2849.
19 S. M. Cui, H. H. Pu, E. C. Mattson, G. H. Lu, S. Mao, M. Weinert, C. J. Hirschmugl, M. Gajdardziska-Josifovska and J. H. Chen, *Nanoscale*, 2012, **4**, 5887.
20 S. M. Cui, E. C. Mattson, G. H. Lu, C. Hirschmugl, M. Gajdardziska-Josifovska and J. H. Chen, *J. Nanopart. Res.*, 2012, **14**, 744.
21 A. Fasolino, J. H. Los and M. I. Katsnelson, *Nat. Mater.*, 2007, **6**, 858.
22 J. Q. Tian, S. Liu, Y. W. Zhang, H. Y. Li, L. Wang, Y. L. Luo, A. M. Asiri, A. O. Al-Youbi and X. P. Sun, *Inorg. Chem.*, 2012, **51**, 4742.
23 J. D. Fowler, M. J. Allen, V. C. Tung, Y. Yang, R. B. Kaner and B. H. Weiller, *ACS Nano*, 2009, **3**, 301.
24 S. Mao, S. M. Cui, G. H. Lu, K. H. Yu, Z. H. Wen and J. H. Chen, *J. Mater. Chem.*, 2012, **22**, 11009.
25 G. H. Lu, L. E. Ocola and J. H. Chen, *Adv. Mater.*, 2009, **21**, 2487.
26 G. H. Lu, K. H. Yu, L. E. Ocola and J. H. Chen, *Chem. Commun.*, 2011, **47**, 7761.
27 G. H. Lu, S. Park, K. H. Yu, R. S. Ruoff, L. E. Ocola, D. Rosenmann and J. H. Chen, *ACS Nano*, 2011, **5**, 1154.
28 H. Vedala, D. C. Sorescu, G. P. Kotchey and A. Star, *Nano Lett.*, 2011, **11**, 2342.
29 G. H. Lu, L. E. Ocola and J. H. Chen, *Appl. Phys. Lett.*, 2009, **94**, 083111.
30 S. Mao, S. M. Cui, K. H. Yu, Z. H. Wen, G. H. Lu and J. H. Chen, *Nanoscale*, 2012, **4**, 1275.
31 P. A. Russo, N. Donato, S. G. Leonardi, S. Baek, D. E. Conte, G. Neri and N. Pinna, *Angew. Chem., Int. Ed.*, 2012, **51**, 11053.